01 May 2023

Design And Analysis Of Gold-nanowires Based Multi-channel SPR Sensor

Nasir Mahmood Anjum

Farhan Mumtaz
Missouri University of Science and Technology, mfmawan@mst.edu

Muhammad Aqueel Ashraf

Results in Optics 11 (2023) 100397

Contents lists available at ScienceDirect

Results in Optics

journal homepage: www.sciencedirect.com/journal/results-in-optics

Design and analysis of Gold-nanowires based multi-channel SPR sensor

Nasir Mahmood Anjum [b,1], Farhan Mumtaz [a,1,*], Muhammad Aqueel Ashraf [b]

[a] Department of Electrical and Computer Engineering, Missouri University of Science and Technology, Rolla, MO 65409-0040, USA
[b] Department of Electronics, Quaid-i-Azam University, Islamabad 45320, Pakistan

ARTICLE INFO

Keywords:
Plasmon
D-shaped SPR sensor
Extrinsic multi-channel
Three core fiber
Multi-analytes sensing

ABSTRACT

This research reports the simultaneous multi-analyte sensing capabilities of a D-shaped multi-channel surface plasmon resonance (SPR) sensor. Three channels are truncated in a U-shaped pattern at the side-polished surface of the D-shaped three-core fiber. Three Gold-nanowires (AuNWs) are positioned at the bottom of each sensing channel. To examine the SPR sensor's multi-channel characteristics, a finite element method (FEM) is applied. In order to detect a variety of analytes, *y*-polarized modes-multiplexing is used, which offers a sufficient wavelength range. At an infiltrated refractive index (RI) of 1.35, 1.38, and 1.41, respectively, the maximal RI sensitivities of c-1 (channel-one), c-2 (channel-two), and c-3 (channel-three) are found as 7,611 nm/RIU, 5,128 nm/RIU, and 12,974 nm/RIU, respectively. Moreover, the sensing structure with three external sensing channels is being demonstrated first time, to the best of our knowledge, using multicore fiber for the detection and discrimination of three different analytes simultaneously. According to expectations, the proposed sensor may be helpful for the detection of a wide range of chemicals and bio-analytes.

1. Introduction

Due to unique optical, electrical, and mechanical characteristics, gold (Au)-based structures like nanoparticles and nanowires are frequently utilized as the building blocks for sensing devices in the chemistry and biochemistry sectors (Zhang et al., 2014). The superior physiochemical characteristics of AuNWs (Gold nanowires) make them valuable components for nanotechnology. Regarding unique gold nanostructures, ultrathin AuNWs are a great choice for nanoelectrodes in electrochemical applications such pressure sensors, DNA detectors, interconnects, and nanoelectrodes (Dawson and O'Riordan, 2011). AuNWs are able to provide high current densities, an excellent signal-to-noise ratio, and low double layer capacitance due to the surface-location of 70 % of their gold atoms. For sensing applications, these characteristics are crucial due to their superior physical and chemical characteristics, AuNWs and Au-nanoparticles, which range in diameter from 1 nm to 100 nm, are frequently utilized in chemical and biological sensors. One of the reasons why AuNWs are so popular in many scientific domains, particularly in the creation of sensors, is their distinctive optical feature. AuNWs produce significant absorption and scattering of light about 520 nm (Jain et al., 2006), which results from the collective oscillation of conduction electrons on the surface of AuNWs when they are stimulated by the incoming light, is what gives the material its bright color. As a result, the size of AuNWs may be adjusted to alter the SPR peak, and this property cannot be seen in bulk gold or AuNWs less than 2 nm in diameter. Therefore, AuNWs is a strong option for integration into SPR-based optical sensors.

SPR sensors have a number of advantages for the detection of biomolecules (Kumar et al., 2023) because of their high sensitivity, high throughput capabilities, label-free detection, rapid real-time monitoring, and non-destructive studies (Mumtaz et al., 2022; Rifat et al., 2018; Zhang et al., 2019; Cao et al., 2018). Numerous practical applications of common chemicals and biomolecules use SPR sensors for food safety inspection, chronic disease diagnosis, health and environmental monitoring, drug testing, chemical reactions of substances, etc. Traditional SPR sensors exhibit several limitations for detection procedures such as centralized laboratories, technically skilled workers, electronic and optical apparatus for alignment, etc (Liu et al., 2015). To overwhelm the deficiencies accumulated by the traditional SPR sensors, researchers reported miniatured SPR sensors based on fiber-optics, such as single-mode fiber (SMF) based SPR sensors (Liu et al., 2021; Pathak et al., 2021; Kadhim et al., 2022), photonic crystal fiber (PCF)-based SPR sensors (Chen et al., 2018; Haque et al., 2018; Mishra et al., 2020), etc. The PCF-based SPR sensing structures are characterized by internal and

* Corresponding author.
E-mail address: mfmawan@mst.edu (F. Mumtaz).
[1] co-first authors and contributed equally.

https://doi.org/10.1016/j.rio.2023.100397
Received 1 January 2023; Received in revised form 25 January 2023; Accepted 20 February 2023
Available online 24 February 2023

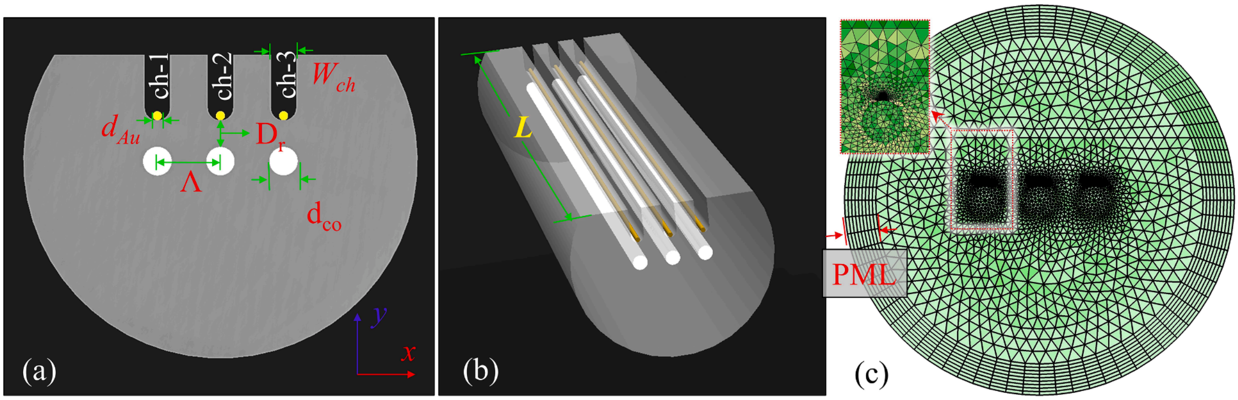

Fig. 1. (a) Transverse, (b) perspective view with geometrical parameters, and (c) mesh profile of the D-shaped multi-channel SPR sensor.

external sensing channels that depend on the positioning of the metal layer corresponding to the generation of a localized plasmonic field. In the SPR sensors, the internal sensing mechanism is much more difficult to realize than that of the external sensing mechanism. Most SPR sensors allow the detection and quantification of only one analyte at a time, but there is a severe need to detect multiple analytes simultaneously. The methods using propagation of *x*-polarized (pol), *y*-pol, or both × and *y*-pol modes are employed to attain multi-analyte sensing. Various chemicals and bio-analytes are simultaneously detected via multi-channel SPR sensors (Cao et al., 2018; Liu et al., 2015; Mishra et al., 2020; Haider et al., 2020; Liu et al., 2016; Yasli et al., 2020; Kaur and Singh, 2019). Liu *et al.* (Liu et al., 2016) explored time-division multiplexing technology via multi-channel structure, presented RI sensitivity is 2,288 nm/RIU ranging from 1.333 to 1.385, although the sensitivity of the sensor is quite low but presented simultaneous sensing tendency of multi-analyte. Prism-based long-range SPRs have been reported for the detection of biomolecules(Singh et al., 2021; Verma et al., 2022), which promoted high imaging sensitivities and improved figure of merit (FOM). Taylor *et al.* (Taylor et al., 2006) reported a prism-based multi-channel SPR sensor that demonstrates the sensing of foodborne bacterial pathogens. The multiplexing capabilities and sensing approach of their SPR sensor are attractive, but the prism-based structure displayed obstacles of tools/settings during procedures (Maurya et al., 2022). Nelson *et al.* (Gomez-Cardona et al., 2020) reported a SPR sensor based on H-shaped microstructured optical fiber whereby presented the highest RI sensitivity of 7540 nm/RIU by using two symmetrical channels for the detection of analytes in the range of 1.33 to 1.39. Yasli *et al.* (Yasli et al., 2020) utilized *x*-pol and *y*-pol modes to demonstrate the performance of a PCF-based SPR sensor, and the obtained RI sensitivities are 2500 nm/RIU and 3083 nm/RIU using c-1 and c-2 in the detection range of 1.33 to 1.36, respectively. An internal multi-channel PCF-based SPR sensor with 2,000 nm/RIU and 18,000 nm/RIU RI sensitivities were presented in ref (Haider et al., 2020) using c-1 and c-2 with y-pol modes propagation, respectively. Whereas c-3 exhibits a RI sensitivity of 3,000 nm/RIU with *x*-pol modes propagation, in the analyte RI range of 1.33 to 1.42. The advantages of the sensor include high RI sensitivity at 1.42 with simultaneous detection of three analytes, and suddenly presents the disadvantage of internal sensing channels that may affect the sensor performance for realization. PCFs are the most widely used in SPR sensors although micro-structuring introduces operational complexities. Additionally, the SPR sensors with multi-channel have unique advantages, such as inexpensive, and rapid detection, which enhance sensing technology.

Influenced by the multi-channel sensing approach, a simple and compact sensing structure is proposed for multi-analyte sensing simultaneously. The sensor is a side-polished D-shaped structure and has three Germanium-doped cores with three external sensing channels. AuNW is placed at the base of each channel in the closed vicinity of the respective adjacent core. The mode coupling demonstrates the multiplexing in the sensing structure, and simultaneously the external sensing channels provide operational simplicity. The sensor effectively demonstrates up-to-the-mark performance using just *y*-pol modes propagation in comparison with earlier reported sensors, those depend on both polarizations for multi-analyte sensing (such as a structure reported in ref. (Haider et al., 2020)). The proposed D-shaped multi-channel SPR sensor certainly has the potential to trade off SPR sensors that are single/dual channel devices and detect two analytes or only one analyte at the same time.

2. Sensor configurations

The schematic cross-sections of the proposed sensor are shown in Fig. 1(a-b). The D-shaped optical fiber consists of three cores, and each core has correspondingly-three adjacent extrinsic sensing channels. The c-1, c-2, and c-3 are U-shaped and have the identical channel width “W_{ch}”. AuNW, which is being employed as a plasmonic material to stimulate SPR (Mumtaz et al., 2023), is positioned at the bottom of each channel. Au-NWs’ diameter is represented by the symbol d_{Au}. The cores and clad diameters of 8.2 μm and 125 μm are used, where the resonance matching condition of the sensor is strongly dependent on the composition of the optical fiber and the plasmonic material. Λ represents the pitch distance between the adjacent cores. D_r is the residual distance from the sensing channel base to the nearest point at the boundary of the corresponding core. The wavelength dependent RIs of D-shaped optical fiber for core (Germanium-doped silica) and cladding (Pure silica) are estimated by (Mumtaz et al., 2022; Mumtaz et al., 2023)

$$n(\lambda) = \sqrt{1 + \frac{\kappa_1\lambda^2}{\lambda^2 - \xi_1^2} + \frac{\kappa_2\lambda^2}{\lambda^2 - \xi_2^2} + \frac{\kappa_3\lambda^2}{\lambda^2 - \xi_3^2}} \quad (1)$$

where, the coefficients of the Sellmeier dispersion equation (i.e., κ_1, κ_2, κ_3, ξ_1, ξ_2, and ξ_3) are given in ref (Mumtaz et al., 2022). The Drude-Lorentz model can be used to determine the material permittivity of Au as (Luo et al., 2021; Gómez-Cardona et al., 2018);

$$\varepsilon_{Au} = \varepsilon_\infty - \frac{\omega_D^2}{\omega(\omega + i\gamma_D)} - \frac{\Delta\varepsilon.\Omega_L^2}{(\omega^2 - \Omega_L^2) + i\Gamma_L\omega} \quad (2)$$

where the values of the Lorentz oscillator strength (Ω_L), spectral width (Γ_L), plasma frequency (ω_D), angular frequency (ω), damping coefficient (γ_D), weighting factor ($\Delta\varepsilon$), and permittivity at high frequency (ε_∞), are shown in reference (Chen et al., 2021).

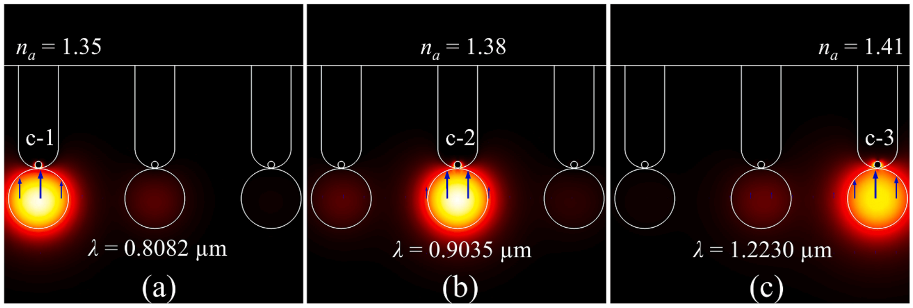

Fig. 2. The electric field distribution of *y*-polarized SPP and fundamental mode coupling constitute phase matching conditions at a certain wavelength for (a) c-1 at $n_a = 1.35$, (b) c-2 at $n_a = 1.38$ and (c) c-3 at $n_a = 1.41$.

3. Results and discussions

3.1. Modal characteristics

The numerical simulation runs to determine the performance of the proposed D-shaped multi-channel SPR sensor. COMSOL Multiphysics 6.0 software is employed to accomplish the numerical solution. The sensor generates surface plasmon polarization (SPP) mode when a certain wavelength is triggered in one channel and the other two remained off. The mesh of the proposed geometry is defined to execute FEM based precise modal solution, and the mesh contains 17 ~ domains, 61 ~ edges, 48 ~ points, and 5874 ~ elements, as shown in Fig. 1(c). Perfect match layer (PML) is employed to absorb the reflections at the boundary interface and the size of PML is 10 % of the cladding diameter. The phase-matching condition in each channel is obtained at a certain wavelength in the SPR sensor when each channel is specified with the corresponding range of RI analytes, as shown in Fig. 2. For example, the electric field of *y*-pol mode exhibit phase-matching conditions and modes-multiplexing is achieved when analyte RI (n_a) at c-1, c-2, and c-3 are infiltrated with 1.35, 1.38, and 1.41. The excitation of SPP mode in c-1, c-2, and c-3 came into being at a certain wavelength, i.e., 0.8082 μm, 0.9635 μm, and 1.2230 μm, for infiltrated n_a value of 1.35, 1.38, and 1.41, as shown in Fig. 2(a-c), respectively.

3.2. Optimization of sensor parameters

Firstly, the optimization of structural parameters is taken into account before the classification of the sensor with a range of RI analytes. The D_r is a key parameter in the lieu of structural optimization for the sensor. The stronger coupling between SPP mode and fundamental mode produces a larger extinction ratio of confinement loss (CL) peak whereby D_r substantially influences the loss spectrum. The spectral CL corresponding to the core-guided mode of the proposed D-shaped multi-channel SPR sensor can be estimated by (Cao et al., 2018);

$$CL = 8.686 \times K_o \mathrm{Im}(n_{eff}) \times 10^4 \, (dB/cm) \quad (3)$$

where, $K_o = 2\pi/\lambda$ (λ denotes the operating wavelength and is taken in μm), and $\mathrm{Im}(n_{eff})$ represents the imaginary part of the effective RI. Comparing the CL for *y*-pol and *x*-pol, it can be seen that the *x*-pol modes exhibit significantly reduced CL in the interference pattern, as seen in Fig. 3. Additionally, the operational wavelength-dependent effective refractive indices for the *y*-pol and *x*-pol propagating modes, which exhibit slight variations in the wavelength range of 1.15 μm to 1.4 μm, were also determined. The demonstrations that follow examine CL's influence in the spectral domain.

Firstly, the CL spectra are obtained with the variation of D_r from 0.1 μm to 0.3 μm. The maximum CL peak value for c-1, c-2, and c-3 are achieved with $D_r = 0.1$ μm where $D_r = 0.2$ μm and 0.3 μm are displayed lesser CL peak values, and n_a is taken as 1.33, 1.36, and 1.39, respectively, as shown in Fig. 4(a). Alternately, the minimal distance from the plasmonic AuNWs to the corresponding core offers stronger mode coupling, interestingly the D_r runs away from the core boundary reduces CL as well as mode coupling, therefore, the optimized value of D_r is considered as 0.1 μm. Another critical parameter is d_{Au} which alters the performance of the SPR sensor. It is observed that the d_{Au} governs the effective RI of SPP modes, varying from 0.8 μm to 1.2 μm finds out CL peaks resonant locations, as shown in Fig. 4(b). The limitations prevailed by the switching of channels as per the range of analytes and in accordance with defined groups, the optimized d_{Au} parameter is considered as 1.0 μm. The Λ demonstrates the coupling phenomena in either the optical fiber functions under strongly or weakly coupled modes. In this.

research, a strongly coupled optical fiber-based SPR sensor is considered, consequently, Λ is set ≤ 20.0 μm (Sakamoto et al., 2017) and varied from 15.0 μm to 20.0 μm to see its impact on the CL spectra, as shown in Fig. 4(c). It is found that Λ at 17.5 μm is found most suitable for each channel in terms of appropriate CL. Lastly, W_{ch} of each channel is varied from 2.0 μm to 5.0 μm. Noticeably, with the increment of W_{ch} decrease the CL which is caused by the diminishing evanescent field interaction with the increasing volume of analytes, as shown in Fig. 4(d). It is observed that the optimum CL peaks are achieved at 2.0 μm, therefore, with consideration of sensing windows for each analyte group and modes multiplexing competence for each channel, the optimized W_{ch} is considered as 3.0 μm. In the process of structural parameters optimization, one parameter among all parameters is varied while the others are presumed to be fixed, therefore, the scrutinizing of parameters (i.e., D_r, d_{Au}, Λ, and W_{ch}) in terms of optimization results in better SPR sensor performances.

3.3. Sensing performance

The wavelength sensitivity (nm/RIU) is an approach to measure the sensing performance of the proposed sensor, and can be estimated by wavelength interrogation technique(Kadhim et al., 2022);

$$S_\lambda = \frac{\Delta\lambda}{\Delta n_a} \quad (4)$$

where Δλ denotes the difference in wavelength, and Δn_a represents the difference in RI. In order to gauge the sensing performance of the SPR sensor, three groups in accordance with the distribution of analytes are defined, such as c-1 measures the analyte variations from 1.33 to 1.35, c-2 measures the analyte variations from 1.36 to 1.38, and c-3 measures the analyte variations from 1.39 to 1.41 (refer to Table 2). Fig. 5(a-c) shows a graphical representation of the spectral evolution for c-1, c-2, and c-3, which.

correspond to changes in n_a from 1.33 to 1.41. As shown in Fig. 5(a), n_a in c-1 varies from 1.33 to 1.35, whereas n_a in c-2 and c-3 remains constant at 1.36 and 1.39, respectively. In this scenario, the CL peak for c-1 is changing corresponding to a shift in n_a values whereas the CL peaks for c-2 and c-3 neither shifted the wavelength position nor affected the c-1CL peak. Thereafter, n_a in c-2 was varied from 1.36 to 1.38, whereas n_a in c-1 and c-3 remained constant at 1.33 and 1.39,

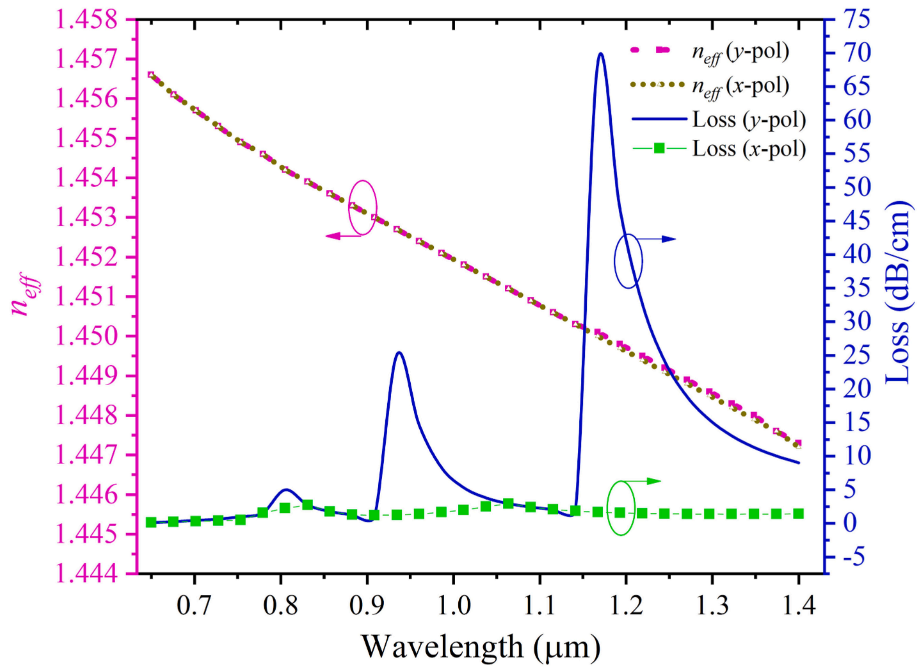

Fig. 3. shows the effective refractive index and confinement loss for the *y*-pol and *x*-pol modes as a function of wavelength, where ch-1, ch-2, and ch-3, respectively, are infiltrated with liquid analyte of 1.35, 1.38, and 1.41.

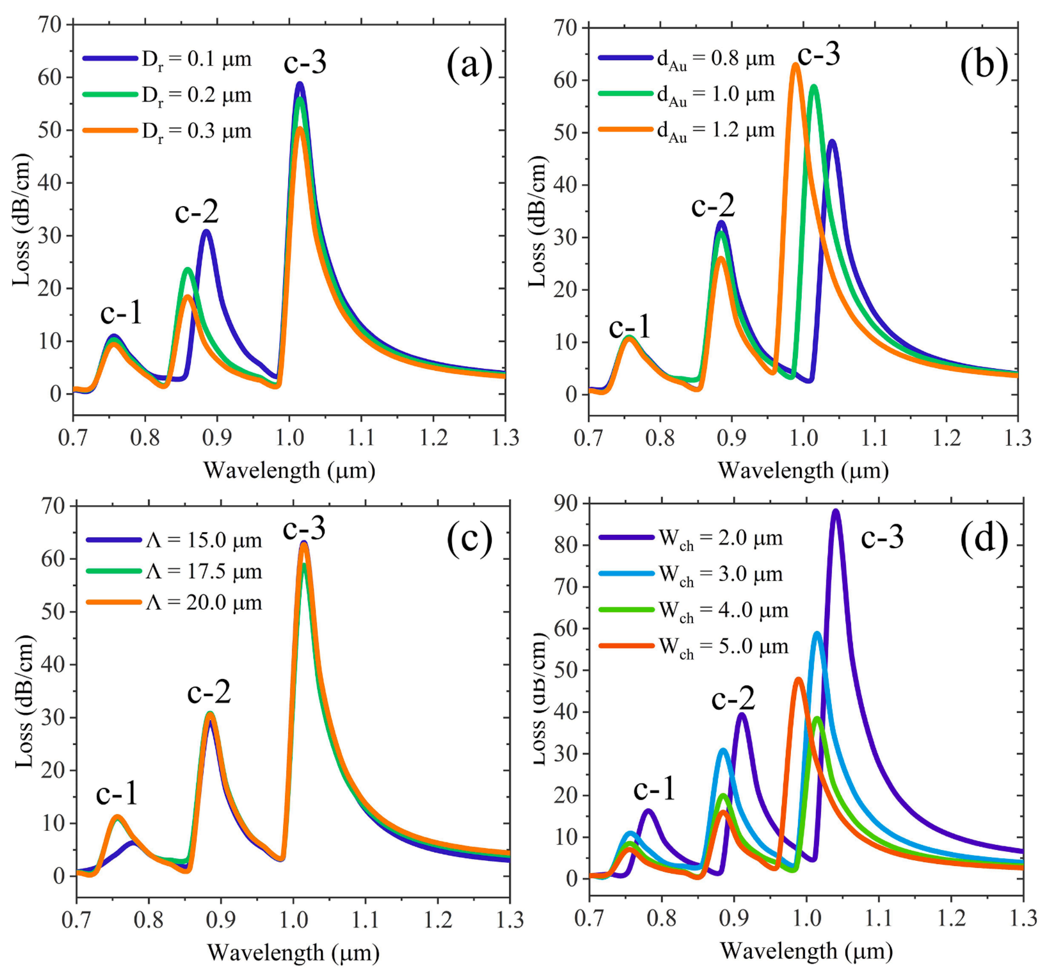

Fig. 4. The structural parameters optimization for the SPR sensor, and the resonance CL peak wavelength for c-1 and c-2 and c-3 shifts as a function of (a) D_r, (b) d_{Au}, (c) Λ, and (d) W_{ch}.

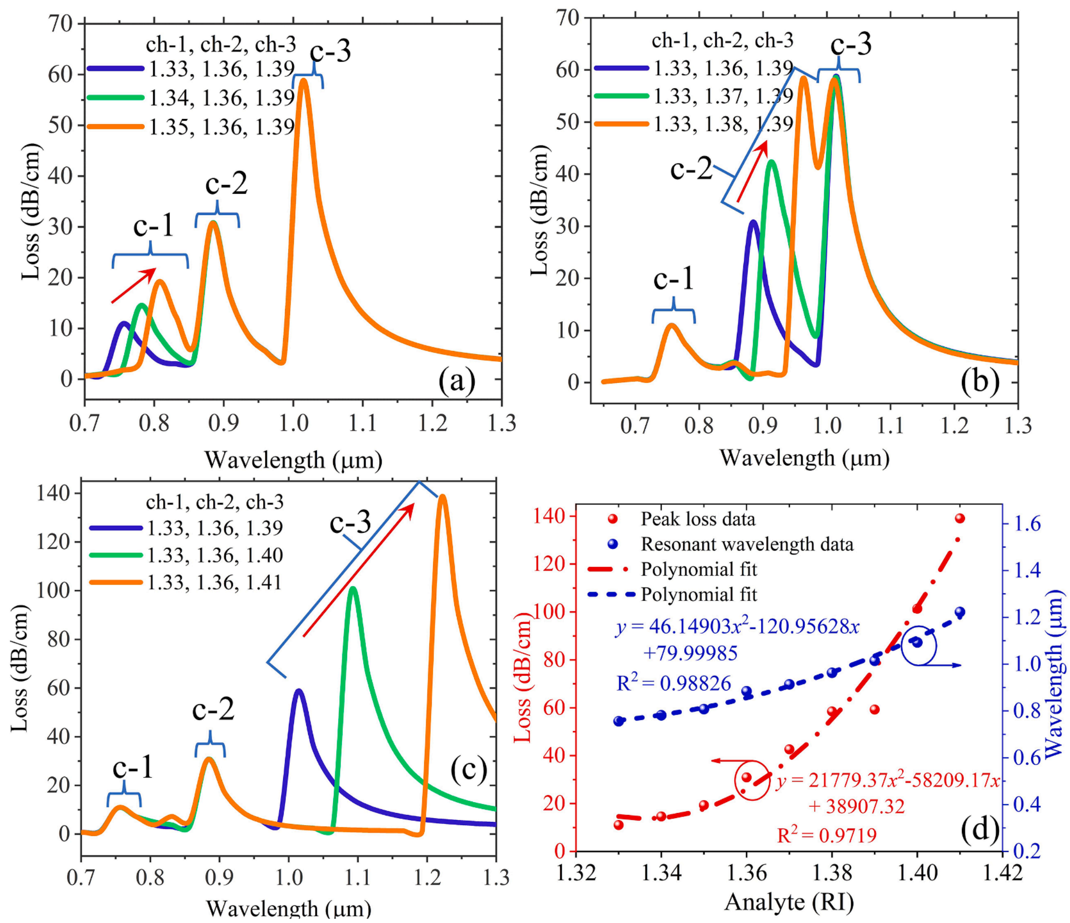

Fig. 5. The SPR sensor CL spectral evolution (a) the n_a in c-1 is varied from 1.33 to 1.35 while other channels remained constant such as c-2 = 1.36 and c-3 = 1.39 (b) the n_a in c-2 is varied from 1.36 to 1.38 while other channels remained constant such as c-1 = 1.33 and c-3 = 1.39 (c) the n_a in c-3 is varied from 1.39 to 1.41 while other channels remained constant such as c-1 = 1.33 and c-2 = 1.36 and (d) the fitting correlation function is obtained for peak CL data and wavelength shift data corresponding to the range of analytes i.e. 1.33 to 1.41.

respectively, as shown in Fig. 5(b). Likewise, the c-1 and c-3 infiltrating analytes had no effect on the c-2 in this instance. Finally, n_a in c-3 varies from 1.39 to 1.41, whereas n_a in c-1 and c-2 remains constant at 1.33 and 1.35, respectively, as shown in Fig. 5(c). In this case, the only difference of a large wavelength shift is observed toward a longer wavelength by c-3 in CL peak as compared to c-1 and c-2 while the rest of the sensing mechanism displays an analogous trend. RI sensitivities of 7,611 nm/RIU, 5,128 nm/RIU, and 12,974 nm/RIU are obtained for c-1, c-2, and c-3, respectively. As shown in Fig. 5(d), the sensitivity curves provide an excellent 2nd-order polynomial fitting correlation function for CL peak data ($R^2 = 0.9719$) and wavelength shift data ($R^2 = 0.98826$) in the RI range of 1.33 to 1.41. The suggested multi-channel SPR configuration encourages the use of smart devices with improved sensitivity and minimal analyte capture rates, which lowers analyte waste. The best measurement resolution with c-3 is 7.71×10^{-6} for a 0.1 nm wavelength change at n_a of 1.40. The remaining values of n_a (i.e., 1.33 to 1.39) are reached with a spectral resolution on the order of 10^{-5}, demonstrating the sensor's capacity to pick up minute variations in n_a. Furthermore, based on analysis, the proposed SPR is extremely suitable for the detection of a wide range of known chemicals and bio-analytes, as shown in Table 1.

On the contrary, amplitude sensitivity is another effective way for assessing the sensing performance of the suggested D-shaped multi-channel SPR sensor, which may be determined (Pathak et al., 2021);

$$S_A = -\frac{1}{\mathrm{CL}(\lambda, n_a)} \times \frac{\partial \mathrm{CL}(\lambda, n_a)}{\partial n_a} \quad (5)$$

Table 1
SPR sensor channel-wise targeted analytes.

Sensing channel	Description	RI
c-1	Alcohol, Methyl	1.33
	Deionized water	1.333
	10 % Glucose sol. in water	1.347
	Ether, Milk	1.35
c-2	Propylene, Acetone, Blood cells	1.36
	Hexane, Acetic acid	1.37
	Skin cell	1.36–1.38
c-3	Cancerous blood cells	1.39
	Cancerous cervical cell	1.392
	Breast cancer cell	1.401
	Decane	1.41

Moreover, this approach is inexpensive and comparatively less complex because it is unlikely that an interpolation function is required to calculate the sensitivity. The spectral evolution shows the variation of amplitude sensitivities at the different values of n_a as shown in Fig. 6(a). Using c-1, c-2, and c-3, the optimum amplitude sensitivities are obtained as $-198.3\ \mathrm{RIU}^{-1}$, $-447.1\ \mathrm{RIU}^{-1}$, and $-721.8\ \mathrm{RIU}^{-1}$ corresponding to n_a values of 1.35, 1.38, and 1.40, respectively (refer to Table 2). As seen in Fig. 6(b), the trend of amplitude sensitivity exhibits a superb 2nd-order polynomial fitting correlation function with R2 = 0.9983.

The inverse of overall CL at any n_a can be added up to estimate the sensor length "L", and when the sensor has high CL, it reduces the sensing length, which is mathematically expressed by(Kadhim et al., 2022);

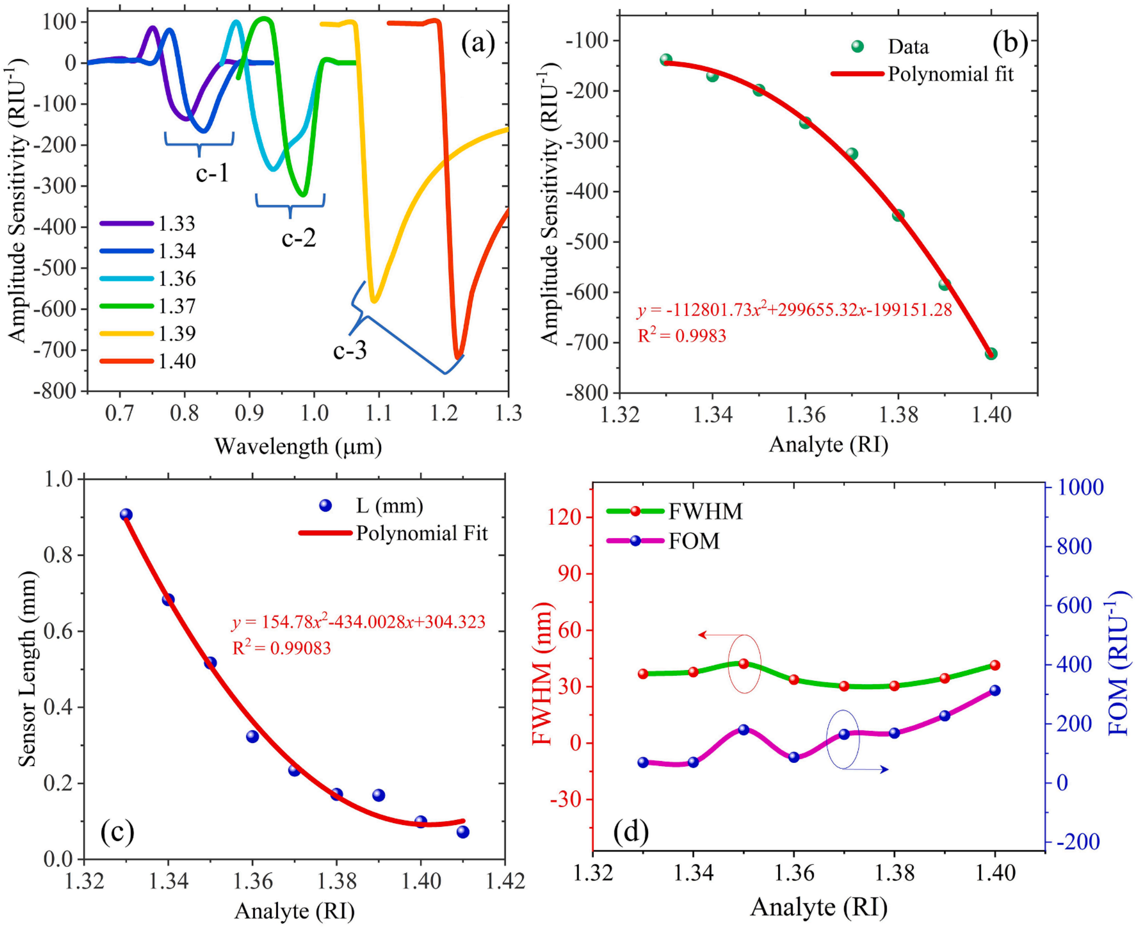

Fig. 6. (a) The spectral evolution shows amplitude sensitivity as a function of the different n_a, polynomial fit correlation function associated with (b) amplitude sensitivity and (c) sensor length, and the trend of (d) FWHM and FOM for the SPR sensor.

Table 2
The sensing performance of the D-shaped multi-channel SPR sensor.

Channel	n_a	S_λ (nm/RIU)	Resolution (RIU)	S_A (RIU^{-1})	FWHM (nm)	FOM (RIU^{-1})
c-1	1.33	2,573	3.89×10^{-5}	−138.0	36.79	69.94
	1.34	2,649	3.78×10^{-5}	−169.9	37.76	70.15
	1.35	7,611	1.31×10^{-5}	−198.3	42.22	180.27
c-2	1.36	2,940	3.40×10^{-5}	−263.1	33.73	87.16
	1.37	4,984	2.01×10^{-5}	−325.1	30.23	164.87
	1.38	5,128	1.95×10^{-5}	−447.1	30.40	168.68
c-3	1.39	7,843	1.28×10^{-5}	−584.2	34.49	227.40
	1.40	12,974	7.71×10^{-6}	−721.8	41.38	313.53
	1.41	N/A	N/A	N/A	38.52	N/A

$$L = -\frac{1}{\mathrm{CL}(\lambda, n_a)} \tag{6}$$

The sensing length is obtained as 0.91 mm, 0.68 mm, 0.52 mm, 0.32 mm, 0.23 mm, 0.17 mm, 0.17 mm, 0.10 mm, and 0.07 mm corresponding to the n_a value of 1.33, 1.34, 1.35, 1.36, 1.37, 1.38, 1.39, 1.40, and 1.41, respectively, as shown in Fig. 6(c). The sensor length tends to decrease as n_a increases, which affirms that the proposed SPR is a miniaturized probe. Other critical parameters for determining the performance of the sensor are full-width half maximum (FWHM) and figure of merit (FOM). The FOM provides information related to the detection capabilities of a sensor, which can be estimated by(Liu et al., 2019);

$$FOM = -\frac{S_\lambda}{FWHM} \tag{7}$$

The full-width half maximum (FWHM) and FOM are displayed in Fig. 6(d). It is obvious that the suggested SPR sensor has a narrow resonance peak that increases with the value of n_a. Thus, a reduction of 3 dB bandwidth or FWHM is obtained. The FWHM is decreased to 38.52 nm at n_a of 1.41. The suggested SPR has an FWHM of 41.38 nm at n_a of 1.40 and a maximum FOM of 313.53 RIU^{-1}. Table 2 shows the obtained FWHM and FOM values corresponding to the n_a. Table 3 compares the performance of the proposed SPR sensor to that of previously reported sensors, demonstrating that the suggested SPR sensor has greater sensitivities, a simple construction, and only uses the y-pol modes sensing technique.

4. Conclusion

In conclusion, a side-polished D-shaped multi-channel SPR sensor for simultaneous multi-analyte detection is suggested and demonstrated. Three-core optical fiber with external multi-channel offers distinct multi-analyte sensing regions. The structural optimization of the sensor is performed by tuning the critical parameters that influence CL spectra. By using wavelength and amplitude interrogation techniques, the sensitivities are acquired. The SPR sensor functions under the y-pol mode propagation that provides a sufficient wavelength tracing span for each channel to detect the targeted analytes in the division of analytes groups. The optimal wavelength and amplitude sensitivities for the SPR sensor with AuNWs structure are 12,974 nm/RIU and 721.28 RIU^{-1} in the analytes RI range of 1.33 to 1.41, respectively. A maximum FOM of 313.53 RIU^{-1} is attained, and it also offers the finest measurement resolution on the order of 10^{-6} RIU^{-1} using the wavelength interrogation

Table 3
Comparative analysis of previously reported multi-channel SPR sensors.

Ref.	SPR design	SPR material	S_λ (nm/RIU)	S_A (RIU-1)	n_a range	Sensing method	Structure
(Kaur and Singh, 2019)	PCF SPR (2-channels)	Au	c-1 ~ 1,000 c-2 ~ 3,750	– –	1.30 to 1.40	1st and 3rd order modes 3rd and 5th order modes	complex
(Liu et al., 2016)	PCF SPR (2-channels)	Au	c-1 ~ 2,500 c-2 ~ 3,083	– –	1.354 to 1.366	x-pol y-pol	complex
(Haider et al., 2020)	PCF SPR (3-channels)	Au	c-1 ~ 2,000 c-2 ~ 3,000 c-3 ~ 18,000	95 184 427	1.33 to 1.35 1.36 to 1.38 1.39 to 1.42	y-pol x-pol y-pol	complex
(Gomez-Cardona et al., 2020)	Multi-channel H-shaped MOF sensor (2- channels)	Au	c-1 ~ 3,300 c-2 ~ 7,540	– –	1.33 to 1.39	y-pol	Simple
This work	D-shaped SPR (3-channels)	Au	c-1 ~ 7,611 c-2 ~ 5,128 c-3 ~ 12,974	−198.35 −325.18 −721.84	1.33 to 1.35 1.36 to 1.38 1.39 to 1.41	y-pol	Simple

approach. The suggested D-shaped multi-channel SPR sensor is expected to be a possible contender in the area of sensing for several biochemical applications based on the sensor's multiplexing abilities and performance.

CRediT authorship contribution statement

Nasir Mahmood Anjum: Methodology, Software, Validation, Writing – original draft. **Farhan Mumtaz:** Conceptualization, Methodology, Software, Validation, Writing – original draft, Project administration, Supervision. **Muhammad Aqueel Ashraf:** Supervision.

Declaration of Competing Interest

The authors declare that they have no known competing financial interests or personal relationships that could have appeared to influence the work reported in this paper.

Data availability

Data will be made available on request.

References

Cao, S., Shao, Y., Wang, Y., Wu, T., Zhang, L., Huang, Y., Zhang, F., Liao, C., He, J., Wang, Y., 2018. Highly sensitive surface plasmon resonance biosensor based on a low-index polymer optical fiber. Optics Express. 26, 3988. https://doi.org/10.1364/oe.26.003988.

Chen, X.i., Bu, W., Wu, Z., Zhang, H., Shum, P.P., Shao, X., Pu, J., 2021. Near-infrared long-range surface plasmon resonance in a D-shaped honeycomb microstructured optical fiber coated with Au film. Optics Express. 29 (11), 16455.

Chen, X., Xia, L., Li, C., 2018. Surface plasmon resonance sensor based on a novel D-shaped photonic crystal fiber for low refractive index detection. IEEE Photonics Journal. 10, 1–9. https://doi.org/10.1109/JPHOT.2018.2790424.

Dawson, K., O'Riordan, A., 2011. Towards nanowire (bio) sensors. Journal of Physics: Conference Series. 307, 012004.

Gómez-Cardona, N.D., Reyes-Vera, E., Torres, P.I., 2018. Multi-Plasmon Resonances in Microstructured Optical Fibers: Extending the Detection Range of SPR Sensors and a Multi-Analyte Sensing Technique. IEEE Sensors Journal. 18, 7492–7498. https://doi.org/10.1109/JSEN.2018.2861709.

Gomez-Cardona, N., Reyes-Vera, E., Torres, P., 2020. High sensitivity refractive index sensor based on the excitation of long-range surface plasmon polaritons in H-shaped optical fiber. Sensors (Switzerland). 20 (7), 2111.

Haider, F., Ahmmed Aoni, R., Ahmed, R., Amouzad Mahdiraji, G., Fahmi Azman, M., Adikan, F.R.M., 2020. Mode-multiplex plasmonic sensor for multi-analyte detection. Optics Letters. 45, 3945. https://doi.org/10.1364/ol.396340.

Haque, E., Hossain, M.A., Ahmed, F., Namihira, Y., 2018. Surface Plasmon Resonance Sensor Based on Modified D-Shaped Photonic Crystal Fiber for Wider Range of Refractive Index Detection. IEEE Sensors Journal. 18, 8287–8293. https://doi.org/10.1109/JSEN.2018.2865514.

Jain, P.K., Lee, K.S., El-Sayed, I.H., El-Sayed, M.A., 2006. Calculated absorption and scattering properties of gold nanoparticles of different size, shape, and composition: Applications in biological imaging and biomedicine. Journal of Physical Chemistry B. 110, 7238–7248. https://doi.org/10.1021/jp057170o.

Kadhim, R.A., Wu, J., Wang, Z., 2022. Sensitivity Enhancement of a Plasmonic Sensor Based on a Side Opening Quasi-D-Shaped Optical Fiber with Au Nanowires. Journal of Optics (India). 51, 71–78. https://doi.org/10.1007/s12596-021-00747-2.

Kaur, V., Singh, S., 2019. A dual-channel surface plasmon resonance biosensor based on a photonic crystal fiber for multianalyte sensing. Journal of Computational Electronics. 18, 319–328. https://doi.org/10.1007/s10825-019-01305-7.

Kumar, S., Singh, R., Wang, Z., Li, M., Liu, X., Zhang, W., Zhang, B., Li, G., 2023. (Invited) Advances in 2D nanomaterials-assisted plasmonics optical fiber sensors for biomolecules detection. Results in Optics. 10 https://doi.org/10.1016/j.rio.2022.100342.

Liu, S., Cao, S., Zhang, Z., Wang, Y., Liao, C., Wang, Y., 2019. Temperature sensor based on side-polished fiber SPR device coated with polymer. Sensors (Switzerland). 19 (19), 4063.

Liu, Y., Chen, S., Liu, Q., Masson, J.-F., Peng, W., 2015. Compact multi-channel surface plasmon resonance sensor for real-time multi-analyte biosensing. Optics Express. 23, 20540. https://doi.org/10.1364/oe.23.020540.

Liu, L., Deng, S., Zheng, J., Yuan, L., Deng, H., Teng, C., 2021. An enhanced plastic optical fiber-based surface plasmon resonance sensor with a double-sided polished structure. Sensors. 21, 1–12. https://doi.org/10.3390/s21041516.

Liu, Z., Wei, Y., Zhang, Y., Wang, Y., Zhao, E., Zhang, Y., Yang, J., Liu, C., Yuan, L., 2016. A multi-channel fiber SPR sensor based on TDM technology, Sensors and Actuators, B. Chemical. 226, 326–331. https://doi.org/10.1016/j.snb.2015.11.102.

Luo, W., Meng, J., Li, X., Xie, Q., Yi, D., Wang, Y., Hong, X., 2021. Temperature effects on surface plasmon resonance sensor based on side-polished D-shaped photonic crystal fiber. Measurement. 181, 109504 https://doi.org/10.1016/j.measurement.2021.109504.

Maurya, P., Maurya, S., Verma, R., 2022. Sensitivity enhancement of SPR based refractive index sensor in VIS-NIR region by using ZnS and PVP. Results in Optics. 8, 100246 https://doi.org/10.1016/j.rio.2022.100246.

Mishra, G.P., Kumar, D., Chaudhary, V.S., Murmu, G., 2020. Cancer cell detection by a heart-shaped dual-core photonic crystal fiber sensor. Applied Optics. 59, 10321. https://doi.org/10.1364/ao.409221.

Mumtaz, F., Roman, M., Zhang, B., Abbas, L.G., Ashraf, M.A., Fiaz, M.A., Dai, Y., Huang, J., 2022. A simple optical fiber SPR sensor with ultra-high sensitivity for dual-parameter measurement. IEEE Photonics Journal. 14, 1–7. https://doi.org/10.1109/JPHOT.2022.3203930.

Mumtaz, F., Roman, M., Zhang, B., Abbas, L.G., Dai, Y., Ashraf, M.A., Fiaz, M.A., Kumar, A., 2022. MXene (Ti3C2Tx) coated highly-sensitive D-shaped photonic crystal fiber based SPR-biosensor. Photonics and Nanostructures - Fundamentals and Applications. 52, 101090 https://doi.org/10.1016/j.photonics.2022.101090.

Mumtaz, F., Zhang, B., Roman, M., Ghulam, L., Aqueel, M., Dai, Y., 2023. Computational study : Windmill-shaped multi-channel SPR sensor for simultaneous detection of multi-analyte. Measurement. 207, 112386 https://doi.org/10.1016/j.measurement.2022.112386.

Mumtaz, F., Yaseen, G., Roman, M., Abbas, L.G., Ashraf, M.A., Fiaz, M.A., Dai, Y., 2023. Numerical analysis of the highly non-linear and ultra-sensitive modified core of a photonic crystal fiber sensor for detection of liquid analytes. Journal of Optical Society of America B. 40 (1), 142.

Pathak, A., Viphavakit, C., Rahman, B.M.A., Singh, V., 2021. A Highly Sensitive SPR Refractive Index Sensor Based on Microfluidic Channel Assisted with Graphene-Ag Composite Nanowire. IEEE Photonics Journal. 13 (2), 1–8.

Rifat, A.A., haider, F., Ahmed, R., Mahdiraji, G.A., Mahamd Adikan, F.R., Miroshnichenko, A.E., 2018. Highly sensitive selectively coated photonic crystal fiber-based plasmonic sensor. Optics Letters. 43 (4), 891.

Sakamoto, T., Mori, T., Wada, M., Yamamoto, T., Yamamoto, F., Nakajima, K., 2017. Strongly-coupled multi-core fiber and its optical characteristics for MIMO transmission systems. Optical Fiber Technology. 35, 8–18. https://doi.org/10.1016/j.yofte.2016.07.010.

Singh, M.K., Verma, V.K., Pal, S., Prajapati, Y.K., Saini, J.P., 2021. Antimonene mediated long-range SPR imaging sensor with ultrahigh imaging sensitivity and figure of merit. Optical Materials. 121, 111484 https://doi.org/10.1016/j.optmat.2021.111484.

Taylor, A.D., Ladd, J., Yu, Q., Chen, S., Homola, J., Jiang, S., 2006. Quantitative and simultaneous detection of four foodborne bacterial pathogens with a multi-channel SPR sensor. Biosensors and Bioelectronics. 22, 752–758. https://doi.org/10.1016/j.bios.2006.03.012.

Verma, V.K., Kumar, R., Pal, S., Prajapati, Y.K., 2022. Highly sensitive MXene-immobilized long range SPR sensor for biomolecule detection. Optical Materials. 133, 112977 https://doi.org/10.1016/j.optmat.2022.112977.

Yasli, A., Ademgil, H., Haxha, S., Aggoun, A., 2020. Multi-Channel Photonic Crystal Fiber Based Surface Plasmon Resonance Sensor for Multi-Analyte Sensing. IEEE Photonics Journal. 12 (1), 1–15.

Zhang, Y., Chu, W., Foroushani, A.D., Wang, H., Li, D., Liu, J., Barrow, C.J., Wang, X., Yang, W., 2014. New gold nanostructures for sensor applications: A review. Materials. 7, 5169–5201. https://doi.org/10.3390/ma7075169.

Zhang, X., Zhu, X.-S., Shi, Y.-W., 2019. Fiber optic surface plasmon resonance sensor based on a silver-coated large-core suspended-core fiber. Optics Letters. 44, 4550. https://doi.org/10.1364/ol.44.004550.